AIAA JOURNAL
Vol. 32, No. 5, May 1994

Structure of Supersonic Jet Flow and Its Radiated Sound

Reda R. Mankbadi,* M. Ehtesham Hayer,† and Louis A. Povinelli‡
NASA Lewis Research Center, Cleveland, Ohio 44135

The present paper explores the use of large-eddy simulations as a tool for predicting noise from first principles. A high-order numerical scheme is used to perform large-eddy simulations of a supersonic jet flow with emphasis on capturing the time-dependent flow structure representing the sound source. The wavelike nature of this structure under random inflow disturbances is demonstrated. This wavelike structure is then enhanced by taking the inflow disturbances to be purely harmonic. Application of Lighthill's theory to calculate the far-field noise, with the sound source obtained from the calculated time-dependent near field, is demonstrated. Alternative approaches to coupling the near-field sound source to the far-field sound are discussed.

I. Introduction

THE recent surge in aeroacoustics research is largely attributed to NASA's efforts to develop a high-speed civil transport plane. The success of the plane is contingent on reducing its jet exhaust noise. In theory, the radiated sound can be directly obtained by solving the full, unsteady, compressible Navier-Stokes equations. However, solving these equations to obtain the noise for the technologically important high-Reynolds-number flows is beyond current computational capabilities. The pioneering acoustic analogy work of Lighthill[1] and later that of Lilley[2] relates the far-field sound to an a priori known sound source. Acoustic analogy provided some physical understanding of the phenomenon and revealed some features consistent with observations. Its major difficulty, however, is that the sound source is given in terms of the time-dependent flow fluctuations. Accurate prediction of these fluctuations requires solving the full, unsteady, compressible Navier-Stokes equations. For recent reviews on the subject refer to Goldstein[3] and Lighthill.[4]

In subsonic jets it is by now well known that the initial, noise-producing region of the jet is dominated by a large-scale organized structure. The fluctuating component can therefore be viewed as being composed of a coherent component and a random component. The coherent component is believed to be more effective than the random component in radiating sound.[5–14] The far-field noise characteristics can thus be calculated by taking the sound source to be dominated by the organized fluctuations. Several attempts have been directed toward calculating the radiation field generated by the large-scale coherent structure. For example, Crighton,[15] Crow,[16] and Ffowcs-Williams and Kempton[17] used analytically integrable but modeled coherent structure sources to calculate the noise. Liu,[18] Mankbadi,[19] and Tam and Morris[20] adopted the view that the large-scale structure can be represented by instability waves. Tam and Morris[20] calculated the noise produced by linear instability waves. Mankbadi and Liu[21] and Mankbadi[22] calculated the radiation field with the coherent structures represented as nonlinear instability waves interacting with the mean flow and the random turbulence. Lighthill's theory is then used to obtain the corresponding sound field. Some of the predictions are consistent with observations and support the view that the coherent structure is the dominant sound source. For instance, the Strouhal number of the measured peak noise is in close agreement with that calculated from the coherent structure emission. The lower frequency sound radiates preferentially in the forward direction, and as the frequency increases, the peak moves toward the lateral direction. The predicted directivity of sound, however, seems to be only in fair agreement with observations.

Rather than using approximate models to describe the sound source (as outlined in the preceding paragraph), we explore in the present work the possibility of obtaining the sound source directly from the time-dependent Navier-Stokes equations. Although direct numerical simulations using Navier-Stokes equations adequately describe the near field, all of the scales of motion cannot be resolved for the high-Reynolds-number flows of practical interest. Therefore, it is appropriate to perform large-eddy simulation (LES) to accurately predict the larger scales of motion while modeling the subgrid-scale turbulence. The sound source is thus given directly in terms of the calculated time-dependent flowfield.

The governing equations and the numerical procedure are given in Sec. II; the results for the flowfield are discussed in Sec. III. The nature and importance of large-scale structures in supersonic jets considered herein are not as clear as they are in the case for subsonic jets (e.g., the results of the linear instability theory indicate a slower growth rate for the disturbances with increasing Mach number[23]). Thus, we first demonstrate in Sec. III.A the wavelike nature of the time-dependent, large-scale structures in natural supersonic jets by taking the inflow disturbances to be completely random. Then, to simulate excited jets in Sec. III.B, we take the inflow disturbances to be purely harmonic, which enhances the large-scale structure and makes it more organized. Section IV addresses the far-field sound calculations. The limitation of directly extending the Navier-Stokes solution domain to the far field is discussed. Approximate application of Lighthill's theory is given to provide some qualitative features of the radiated sound. The difficulties that arise from the noncompactness of the source are highlighted. Alternative approaches of coupling the near-field to the far-field sound are discussed.

II. Large-Eddy Simulation in Computation of Supersonic Jet Noise

The objective here is to demonstrate the approach rather than to compare it with experimental results. As such, we restrict the analysis to axisymmetric disturbances. This considerably simplifies the process. In supersonic jets, however, the three-dimensional disturbances (helical modes) are expected to be more amplified than the axisymmetric ones. The present results thus cannot be compared quantitatively with experiment, and only qualitative agreement will be discussed. For axisymmetric flow the filtered Navier-

Presented as Paper 93-0549 at the AIAA 31st Aerospace Sciences Meeting, Reno, NV, Jan. 11–14, 1993; received March 1, 1993; revision received Oct. 21, 1993; accepted for publication Oct. 22, 1993.

*Senior Scientist, Leader, Computational Aeroacoustics. Associate Fellow AIAA.

†Senior Research Associate, Institute for Computational Mechanics in Propulsion.

‡Acting Division Chief, Internal Fluid Mechanics Division. Fellow AIAA.

Stokes equations (e.g., Moin et al.[24]) are written in polar coordinates as

$$\frac{\partial Q}{\partial t} + \frac{\partial F}{\partial x} + \frac{1}{r}\frac{\partial (rG)}{\partial r} = S \tag{1}$$

$$Q = \begin{bmatrix} \bar{\rho} \\ \bar{\rho}\tilde{u} \\ \bar{\rho}\tilde{v} \\ \bar{\rho}\tilde{e} \end{bmatrix} \tag{2}$$

$$F = \begin{bmatrix} \bar{\rho}\tilde{u} \\ \bar{p} + \bar{\rho}\tilde{u}^2 - \tau_{xx} \\ \bar{\rho}\tilde{u}\tilde{v} - \tau_{xr} \\ \bar{\rho}\tilde{u}\tilde{I} - \tilde{u}\tau_{xx} - \tilde{v}\tau_{xr} - k\tilde{T}_x \end{bmatrix} \tag{3}$$

$$G = \begin{bmatrix} \bar{\rho}\tilde{v} \\ \bar{\rho}\tilde{u}\tilde{v} - \tau_{xr} \\ \bar{p} + \rho\tilde{v}^2 - \tau_{rr} \\ \bar{\rho}\tilde{v}\tilde{I} - \tilde{u}\tau_{xr} - \tilde{v}\tau_{rr} - k\tilde{T}_r \end{bmatrix} \tag{4}$$

$$S = \frac{1}{r}\begin{bmatrix} 0 \\ 0 \\ \bar{p} - \bar{\tau}_{\theta\theta} \\ 0 \end{bmatrix} \tag{5}$$

Here $\boldsymbol{Q}$ is the unknown vector; F and G are the fluxes in the x and r directions, respectively; and S is the source term. An overbar denotes a filtered quantity, a double overbar denotes time averaging, and a tilde denotes Favre averaging,

$$\tilde{f} = \bar{\rho} f / \bar{\rho} \tag{6}$$

and τ_{ij} are the shear stresses, which are split as

$$\tau = \bar{\tau}_v + \tau_t \tag{7}$$

The subscript v denotes the viscous part, and the subscript t denotes the unresolved turbulent part that needs to be modeled.

A. Modeling Subgrid-Scale Turbulence

In LES the governing equations are filtered for a certain length scale, resulting in the residual turbulent stresses $\tau_{ij,r}$. It might be possible to perform such simulations with no explicit residual turbulence model at all (e.g., Tsuboi et al.[25]). In this case the "numerics" are the dissipative mechanism that sets the smallest scale, and there is no relation between the numerical viscosity and the fluid viscosity. Hussaini et al.[26] warns that "this approach simply cannot predict important Reynolds number effects and consequently should be used with caution."

In the results presented herein, Smagorinsky's[27] model is used. The subgrid-scale turbulence–stresses are modeled as

$$\tau_{t,ij} = q_R^2 \delta_{ij}/3 - 2\rho\nu_R S_{ij} \tag{8}$$

where q_R^2 is the energy of the residual turbulence, which is neglected with respect to the thermodynamic pressure (see Erlebacher et al.[28]); the strain rate of the resolved scale is given by

$$S_{ij} = \frac{1}{2}\left(\frac{\partial \tilde{u}_i}{\partial x_j} + \frac{\partial \tilde{u}_j}{\partial x_i}\right) \tag{9}$$

and ν_R is the effective viscosity of the residual field. Here we take from Hussaini et al.[26]

$$\nu_R = (C_S\Delta)^2\sqrt{2S_{mn}S_{mn}} \tag{10}$$

where $C_s = 0.23$, and Δ is the filter width given by

$$\Delta = (\Delta_x\Delta_r)^{1/2} \tag{11}$$

B. Discretization

As will be demonstrated in Sec. IV the radiated sound is actually a small quantity that is the net cancellation of the sound source after integration over its streamwise extent. Numerical errors should therefore be much smaller than this quantity, and the use of a high-order scheme appears necessary. Spectral methods are highly accurate but cannot resolve shock waves in supersonic flows and lead to oscillations. The discretization scheme used here is an extension of the MacCormack scheme to fourth-order accuracy in space and second-order accuracy in time and is known as the 2–4 scheme.[29] This scheme has also been successfully used before by Farouk et al.[30] and Ragab and Sheen[31] for studying nonlinear instability problems in plane shear layers. The main advantage of the scheme is that it is explicit. An operator splitting is used to maintain the 2–4 accuracy, namely,

$$Q^{n+2} = L_x L_r L_r L_x Q^n \tag{12}$$

where L_x and L_r are one-dimensional solution operators corresponding to the scheme applied to the equations

$$Q_t = F_x, \qquad Q_t = G_r + S \tag{13}$$

respectively, as

$$Q_{ij}^{n+1/2} = Q_{ij}^n + \frac{\Delta t}{6\Delta r}[7(G_{i,j+1} - G_{ij}) - (G_{i,j+2} - G_{i,j+1})]^n + \Delta t S_{ij}^n \tag{14}$$

$$Q_{ij}^{n+1} = \frac{1}{2}\left\{Q_{ij}^{n+1/2} + Q_{ij}^n + \frac{\Delta t}{6\Delta r}[7(G_{ij} - G_{i,j-1}) - (G_{i,j-1} - G_{i,j-2})]^{n+1/2} + \Delta t S_{ij}^{n+1/2}\right\} \tag{15}$$

$$Q_{ij}^{n+3/2} = Q_{ij}^{n+1} + \frac{\Delta t}{6\Delta r}[7(G_{ij} - G_{i,j-1}) - (G_{i,j-1} - G_{i,j-2})]^{n+1} + \Delta t S_{ij}^{n+1} \tag{16}$$

$$Q_{ij}^{n+2} = \frac{1}{2}\left\{Q^{n+1} + Q^{n+3/2} + \frac{\Delta t}{6\Delta r}[7(G_{i,j+1} - G_{ij}) - (G_{i,j+2} - G_{i,j+1})]^{n+3/2} + \Delta t S_{ij}^{n+3/2}\right\} \tag{17}$$

Similar equations can be written for the flux F.

C. Boundary Conditions

The outer-flow boundary conditions need special attention, not only to make the flow numerically stable, but also because they must permit the unsteady flow properties to pass without producing nonphysical reflections. Artificial reflections from applying the boundary conditions, or from suppressing or amplifying the

acoustic feature in the near field, could result in large errors in the predicted far-field sound. This issue is especially critical in the coupling of the near-field solution with the acoustic field solution. We explored several boundary conditions (see Scott et al.[32]), such as Giles,[33] Tam and Webb,[34] and Thompson,[35] but for the results presented herein, little gain was obtained over using Thompson's, which is adopted here.

The MacCormack 2–4 scheme uses one-sided differences of the fluxes. For a computational domain extending from $i = 1$ to m, fluxes are needed at $m+1$, $m+2$, $m-1$ in addition to the interior points. The fluxes at points outside the computational domain are obtained by using cubic extrapolation from the interior, that is,

$$G_{m+1} = 4G_m - 6G_{m-1} + 4G_{m-2} - G_{m-3}$$
$$G_{m+2} = 4G_{m+1} - 6G_m + 4G_{m-1} - G_{m-2} \tag{18}$$

Physical boundary conditions for the computation are derived by using linearized characteristics,

$$P_t - \rho c u_t = \gamma_1$$
$$P_t + \rho c u_t = \gamma_2$$
$$P_t - c^2 \rho_t = \gamma_3 \tag{19}$$
$$v_t = \gamma_4$$

The right-hand sides of Eqs. (18) and (19) are calculated from the solution obtained by applying the scheme at the boundaries. For supersonic flows all characteristics travel in the flow direction. Flow variables are updated at the boundaries by using corrected values of the temporal derivatives. Equations (19) are then solved to get corrected temporal derivatives at the boundary. For subsonic outflows one characteristic variable propagates against the flow direction, but the rest follow the flow direction. For nonreflecting conditions γ_1 is set to zero. The top flow (Fig. 1) is always subsonic normal to the boundary. Symmetry boundary conditions are applied at the jet centerline, where a new set of equations is derived from the original equations by using L'Hospital's rule to circumvent numerical problems associated with geometric singularity in the formulation.

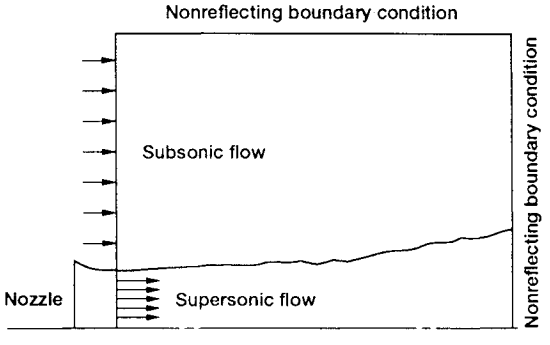

Fig. 1 Computational domain.

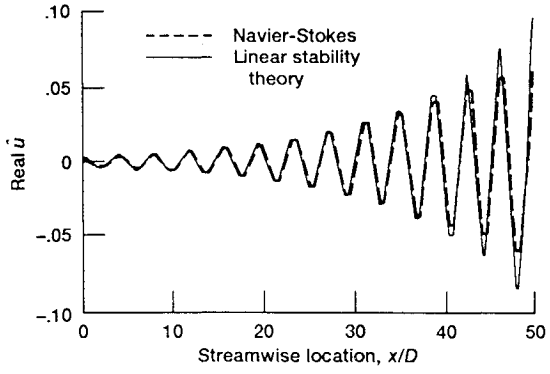

Fig. 2 Comparison between predicted growth of disturbance and linear stability theory.

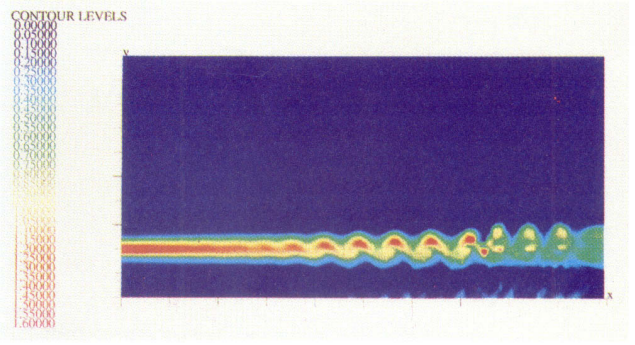

Fig. 3 Snapshot of vorticity field for random disturbance input.

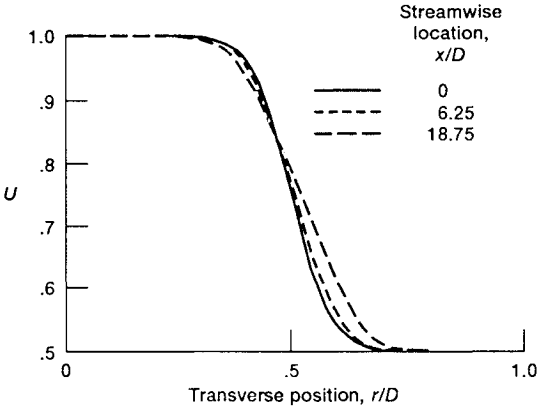

Fig. 4 Radial profile of time-averaged axial velocity.

For subsonic inflow three characteristic variables are specified, and the other one is extrapolated and then corrected as discussed previously. For supersonic inflow all variables are given. The inflow, time-averaged axial velocity profile is given by the hyperbolic tangent

$$\bar{\bar{u}}(y) = 1/2\,\{\,(1+u_\infty) - (1-u_\infty)\tanh[a(r-1)]\,\} \tag{20}$$

where a was taken as 6 (which corresponds to a momentum thickness $\delta_m = 0.0028$ of the jet exit diameter).

D. Code Validation

Because in computational aeroacoustics the oscillatory flowfield is needed, it is necessary to validate not only the time-averaged quantities but also the time-harmonic ones. This was done by perturbing the inflow with a small disturbance, $\varepsilon \sin \omega t$, and then examining its downstream development. According to the linear stability theory, the input disturbance can be either amplified or suppressed, depending on its frequency. A typical comparison between the calculated development of the disturbance and that predicted by the linear stability theory is given in Fig. 2. The flow first goes through an adjustment (receptivity) region because the profile of the input disturbance does not match the eigenfunction (i.e., does not satisfy the linearized form of the Navier-Stokes equation). Following this region the agreement is satisfactory. As the amplitude of the disturbance becomes large, the linear stability theory is no longer valid, and the Navier-Stokes solution begins to deviate from that of the linear stability theory.

III. Results for Flowfield

The disturbances in the inflow usually have random and harmonic components. Results are presented herein with emphasis on

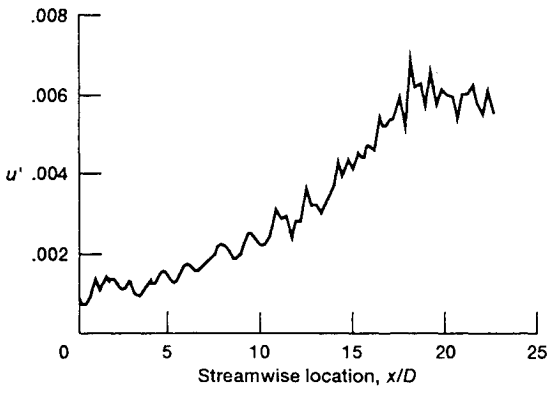

Fig. 5 Root-mean-square value of u' at $r = D/2$.

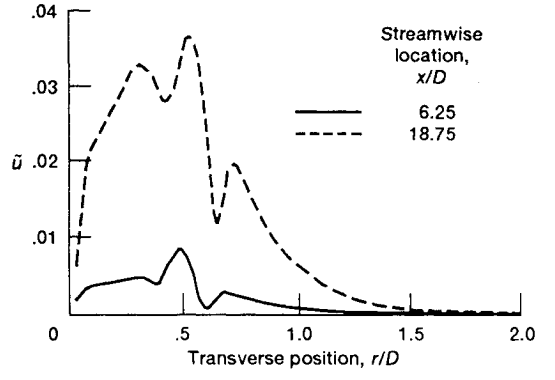

Fig. 6 Profile of turbulence intensity.

two particular types of disturbances: completely random or completely harmonic. The objectives of the first case are to demonstrate the wavelike nature of the large-scale structure, even if the inflow disturbance is completely random, and to show the ability of the numerical scheme to capture this feature of the flow. In the second case, wherein the input disturbances are completely harmonic, the large-scale structure is enhanced, making it easier to examine the results.

The exit Mach number was taken as 1.5, the jet velocity ratio $u_\infty/u_0 = 0.50$, and the temperature ratio $T_\infty/T_0 = 2$. The Reynolds number based on the jet diameter and the inlet velocity was 1.27×10^6. For both cases the computational domain extended 2.5 diameters in the radial direction. For the random inflow case the computational domain extended 25 diameters in the x direction, with a mesh size of 180×125 in x and r. In the harmonic inflow case, to facilitate noise analysis, the computational domain extended 50 diameters in the x direction, with a mesh size of 400×110. The computation started with a time step such that the Courant-Friedrichs-Lewy (CFL) number was 0.3, and later a finer time step was used ($\Delta t = 2^{-9}$, CFL = 0.002) for data analysis. The mesh was uniform in x and stretched in the r direction with the grid points concentrated around $r = D/2$. The calculated signal was stored for the last 128 steps and then time averaged. Subtracting the time-averaged quantities from the instantaneous quantities gave the fluctuating component.

A. Random Inflow Disturbance

Random disturbance was imposed on the inflow in the form

$$\tilde{u} = \bar{\tilde{u}}\,(1 + \varepsilon \mathfrak{F}(t)) \tag{21}$$

where $\mathfrak{F}$ is a computer-generated random function and ε is taken as 0.005. Figure 3 shows a snapshot of the vorticity field, and the "cat's eye" structure is evident in the figure.

The time-averaged streamwise velocity component as shown in Fig. 4 indicates slow spreading of the jet. The development of the rms value of u' at $r = D/2$, shown in Fig. 5, can be taken as a measure of the turbulence intensity, which increases along the jet and then reaches a peak value. The corresponding profile of u', shown in Fig. 6, indicates that the turbulence intensity is maximum around the center of the shear layer.

The total shear stresses, which are composed of the resolved part, and the modeled part are shown in Fig. 7. The stresses were found to be dominated by the resolved part, with the modeled stresses contributing only about 5%. These results are consistent with the observations of Hussaini et al.[26] The shear stress τ_{xx} is dominant, as Fig. 7 indicates.

The spectra of the velocity signal shown in Fig. 8 resemble those of Seiner and Norum.[36] Fast Fourier transform was applied to the time history of a given flow variable, and the real part of the resulting Fourier transform at a given frequency was denoted by a hat. The results are shown in Fig. 9 for the streamwise velocity $\hat{u}$, where the wavelike feature of the structure is quite evident. Because the inflow disturbances were random in this case, there were no well-defined peaks in the spectra, and the development of the predicted structure cannot easily be related to linear or nonlinear theories on instability waves. As described in the next section, when harmonic inflow disturbances were imposed, the structure became more organized, the spectrum had well-defined peaks, and the resemblance to instability waves became evident.

B. Harmonic Excitation

In this case the inflow disturbances were taken to be harmonics in the form

$$\tilde{u} = \bar{\tilde{u}} + \varepsilon e^{-(r-1)^2} \sum_{k=1}^{16} \sin k\omega_f t \tag{22}$$

where ω_f was taken as $\pi/8$ and $\varepsilon = 0.005$. The Gaussian profile of the disturbance was introduced to reduce the initial adjustment zone. Figure 10 shows a snapshot of the instantaneous flowfield.

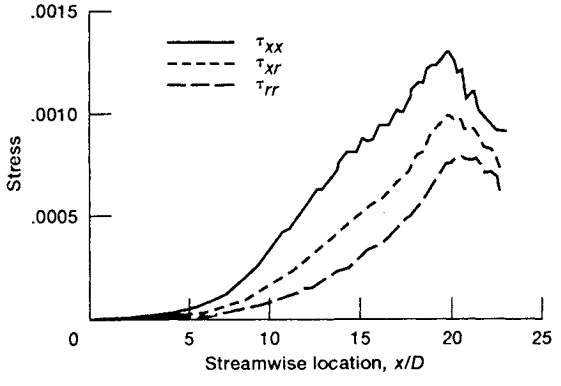

Fig. 7 Axial variation of shear stresses at $r = D/2$.

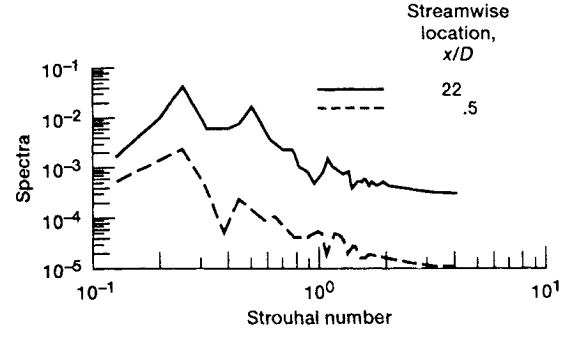

Fig. 8 Spectra of streamwise velocity at $r = D/2$ and $x/D = 22$ and 0.5.

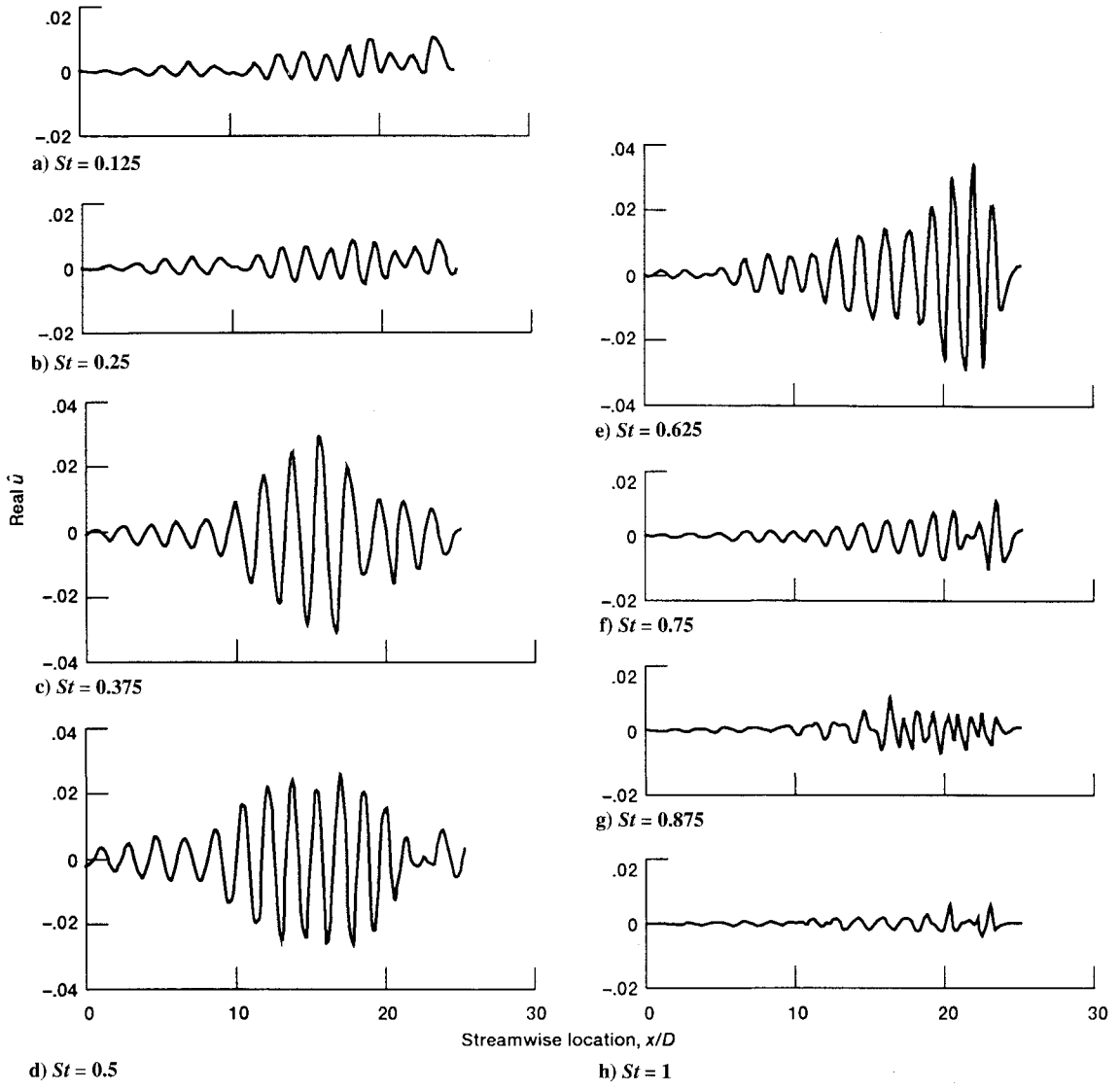

Fig. 9 Real parts of $\hat{u}$ at several Strouhal numbers under random input disturbances.

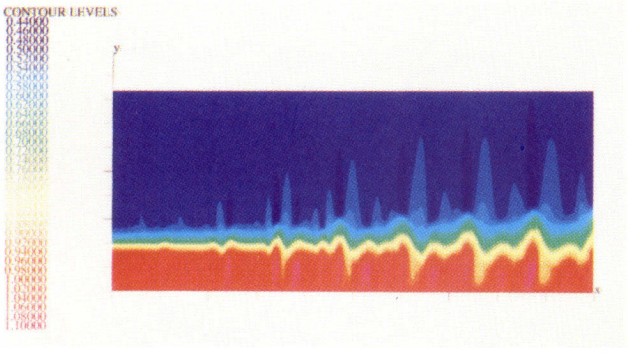

Fig. 10 Snapshot of axial velocity for harmonic inflow disturbance.

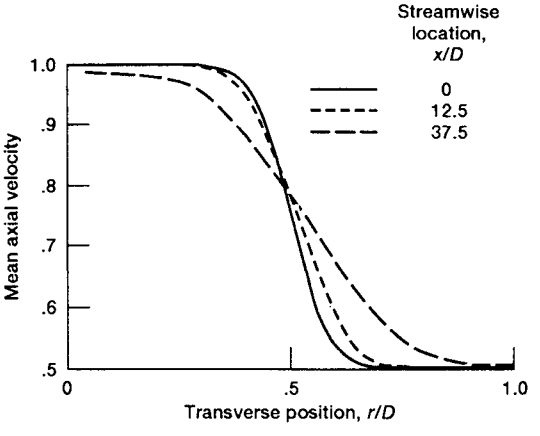

Fig. 11 Radial profile of axial velocity.

The time-averaged streamwise velocity component, shown in Fig. 11, indicates spreading jet. Figure 12 shows that the centerline, time-averaged streamwise velocity decreased in the downstream direction. The results of Figs. 11 and 12 are in good agreement with the numerical simulation of Scott[37] and in qualitative agreement with the experimental observations of Seiner and Norum.[36] But the predicted spreading rate is underestimated in comparison with the experimentally observed ones. The centerline decay here begins to occur at x/D = 20–25, whereas in the experiment (Seiner et al.[38] and Yamamoto et al.[39]) the decay began at about x/D = 10–15. Our calculations indicate that the jet spreading became larger when the Reynolds number was reduced or when the initial disturbance level was increased. However, the most pronounced effect on the spreading rate resulted from taking small initial momentum thickness [larger a in Eq. (20)]. This made the mean-flow velocity gradient sharper and provided energy for the growth of disturbances. Furthermore, the computations here were restricted to the two-dimensional case, but because the three-dimensional effects are known to be quite important, larger spreading rates are expected when the three-dimensional effects are accounted for.

The profile of $\tilde{u}$, shown in Fig. 13, indicates that for small x there is a well-defined peak in the profile around the lip line ($r = D/2$). This peak becomes flat in the downstream direction. This feature is in agreement with the experimental observations (e.g., see Troutt and McLaughlin[40]).

The spectra of the velocity signal are shown in Fig. 14. Well-defined peaks in the spectra correspond to the frequency of the inflow harmonic disturbances. The Fourier components of $\hat{u}$ at a given frequency are shown in Fig. 15. The wavelike feature of the structure is quite evident in the figure. The development of the disturbance amplitude along the jet is shown in Fig. 16 for several Strouhal numbers. The figure indicates a range of Strouhal numbers between 0 and 1.0 where the corresponding amplitudes are higher than the rest. Within this frequency range the higher frequency disturbances peaked closer to the jet exit, and the lower frequency ones peaked farther downstream, which is consistent with Troutt and McLaughlin's[40] measurements. At downstream locations the modes became large and of comparable magnitude. A given mode could begin to decay and then amplify again, possibly because of strong nonlinear interactions between the modes (e.g., see Drubka et al.,[41] Corke and Kusek,[42] Corke et al.,[43] and Mankbadi[44,45]).

IV. Radiated Sound

In principle, one can directly obtain the sound field by extending the solution domain to the far field. However, this requires storage capabilities beyond those currently available. Obtaining the far field directly by using the full Navier-Stokes equations requires a computational domain of about $x = 100D$ and $r = 100D$, with accurate resolution for the near field. As a trial case we submitted a job to the Cray Y-MP with a grid size of 750×300. This size just fits into the 30-megaword storage limitation. The domain size was taken as $x = 75D$ and $r = 15D$. The job advanced a few time steps (from 32.445 to 37.860) in about 3 h of central processing unit (CPU) time. We estimated the job would take an impractically long 200 h of CPU time to complete. Furthermore, the results for the near field may not be accurate enough, the computational domain is not large enough for the calculated pressure to correspond to the far-field sound, and no storage is left for data processing.

The alternative is either to use acoustic analogy to obtain the far field or to patch the resulting near field to a linearized-Euler-equation solution for the far field. We discuss here applying Lighthill's theory to obtain the far-field sound.

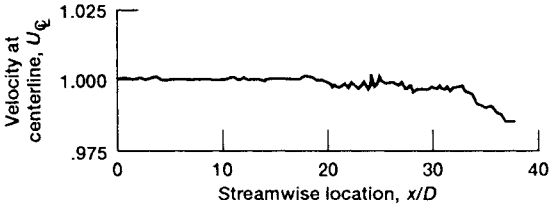

Fig. 12 Streamwise variation of centerline velocity.

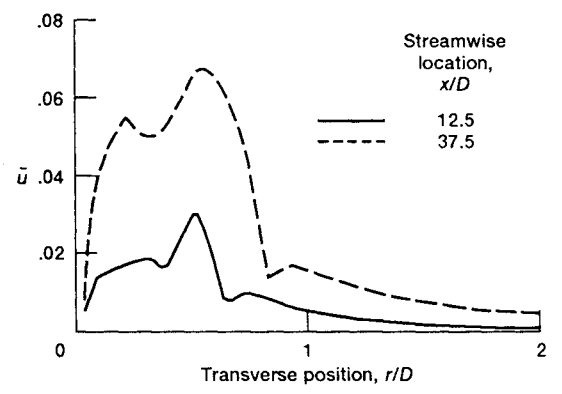

Fig. 13 Profile of $\tilde{u}$.

In Lighthill's theory the far-field sound pressure is given by the volume integral

$$P_s = \frac{1}{4\pi R_{ob} a_0^2} \iiint \left[\frac{\partial^2}{\partial x_i \partial x_j} \{\rho u_i u_j\} + \frac{1}{a_0^2} \frac{\partial^2}{\partial t^2} \{p - a_0^2 \rho\} \right] dV \tag{23}$$

The second source term in Eq. (23) is usually neglected. Here, P_s is the far-field sound pressure, u_i is the velocity vector, a_0 is the speed of sound in the medium surrounding the flow, and R_{ob} is the distance between the jet exit centerline and the observation point. The braces denote that the source term is calculated at the retarded time

$$t_r = t - |\bar{X} - \bar{Y}|/a_0 \tag{24}$$

where X and Y are the observer's and the source's locations, respectively. Accurately accounting for the retarded-time effect would require storing data for an extensive time history, which is beyond current computer capability. An approximation to Lighthill's theory that is usually adopted is to assume the source to be compact and approximate [Eqs. (23) and (24)] as

$$P_s = \frac{1}{4\pi R_{ob} a_0^2} \iiint \frac{\partial^2}{\partial t^2} (\rho c_r^2)\, r\, dr\, dx\, d\phi \tag{25}$$

$$t_r = t - R_{ob}/a_0 + (x \cos\theta + r \sin\theta \cos\phi)/a_0 \tag{26}$$

where

$$C_r = u \cos\theta + v \sin\theta \cos\phi \tag{27}$$

and where θ is the emission angle, and ϕ is the azimuthal angle. Equation (25) can now be written as

$$P_s = \frac{1}{4\pi R_{ob} a_0^2} \iiint \frac{\partial^2}{\partial t^2} [\rho(u^2 \cos\theta^2 + uv \sin 2\theta \cos\phi + v^2 \sin^2\theta \cos^2\phi)] r\, dr\, dx\, d\phi \tag{28}$$

The source term can be decomposed into frequency components as

$$\begin{aligned} \rho uu &= \sum_{k=0} F_{xx}(x, r, \omega_k)\, e^{-i\omega_k t} + \text{c.c.} \\ \rho uv &= \sum_{k=0} F_{xr}(x, r, \omega_k)\, e^{-i\omega_k t} + \text{c.c.} \\ \rho vv &= \sum_{k=0} F_{rr}(x, r, \omega_k)\, e^{-i\omega_k t} + \text{c.c.} \end{aligned} \tag{29}$$

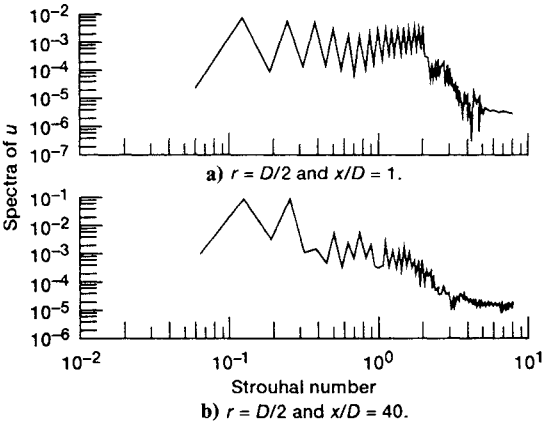

Fig. 14 Spectra of streamwise velocity.

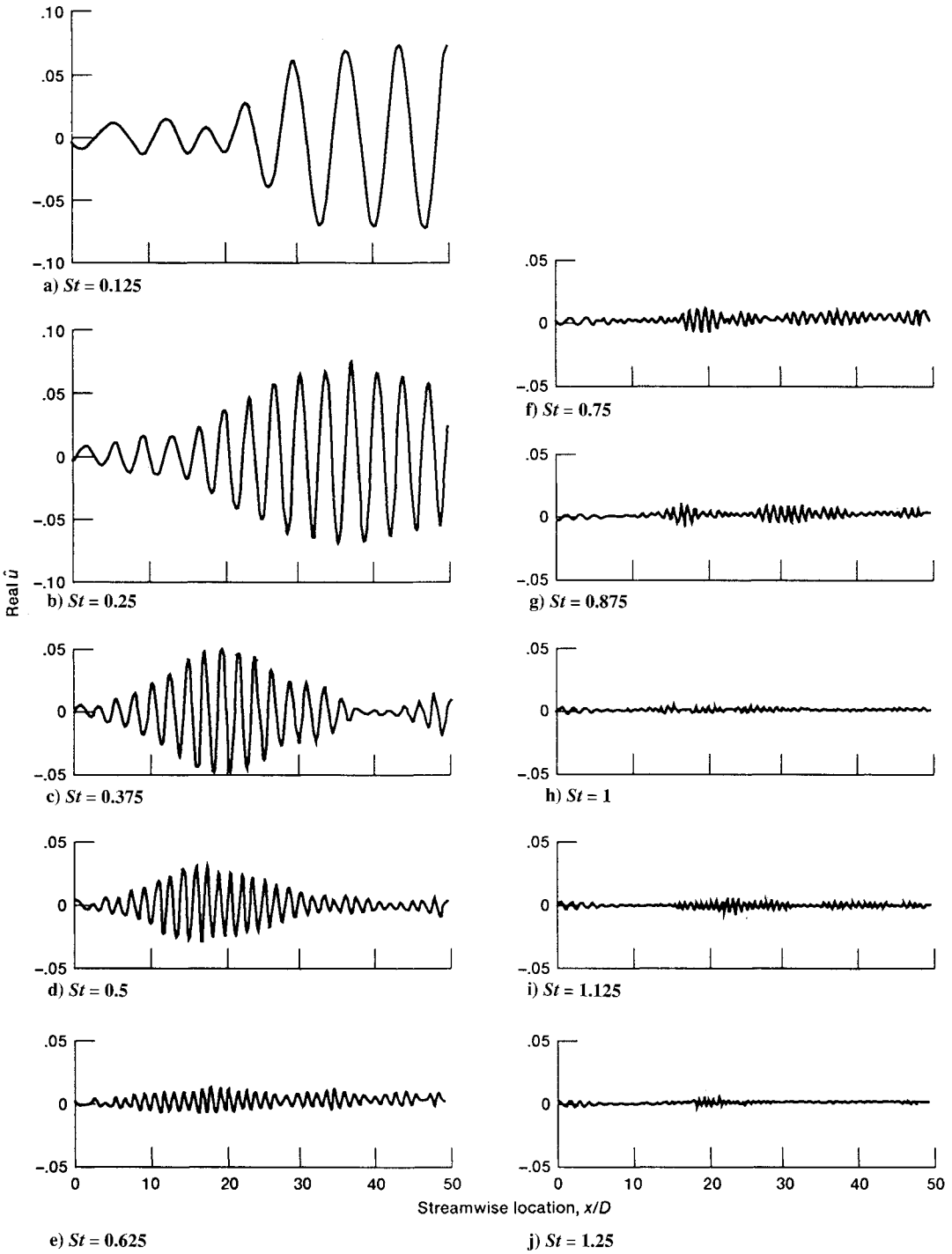

Fig. 15 Real part of $\hat{u}$ at several Strouhal numbers under harmonic input disturbance.

where c.c. denotes the complex conjugate. Figure 17 shows the Fourier transform of ρuu at $St = 0.5$. The streamwise oscillation is evident in the figure.

The sound intensity I is defined as

$$I = \left| P_s / \rho_e a_0^2 \right|^2 \tag{30}$$

Equation (29) is substituted into Eq. (28), and the azimuthal integral is performed. After straightforward manipulation, the far-field sound intensity is obtained as

$$I = C \left| \iint F(x, r, St) \exp\left(-2\pi i M_j St x \cos\theta\right) r \, dr \, dx \right|^2 \tag{31}$$

where

$$C = \frac{\pi}{(R_{ob}/D)^2} St^4 (U_e/a_0)^8 \tag{32}$$

$$F(x, r, St) = A_0 J_0(\sigma) - iA_1 J_1(\sigma) - A_2 J_2(\sigma) \tag{33}$$

$$A_0 = F_{xx} \cos^2\theta + (1/2) F_{rr} \sin^2\theta$$

$$A_1 = F_{xr} \sin 2\theta \tag{34}$$

$$A_2 = (1/2) F_{rr} \sin^2\theta$$

and J is the Bessel function of the argument

$$\sigma = 2\pi StMr \sin\theta \tag{35}$$

The integrand of Eq. (31) represents the sound source at a given Strouhal number as seen by an observer at θ. This sound field is shown in Fig. 18 for $\theta = 30$ deg and $St = 0.5$. The source oscillates between positive and negative along the jet. It extends a few diameters in the transverse direction but a considerable distance in the streamwise direction.

Figure 19 shows the directivity of sound calculated according to Eq. (31) for $St = 0.5$. The nature of the sound field depends on the relative contribution of each term in Eq. (31), which varies with Strouhal number, among other parameters. In Fig. 19 the directivity resembles that of a lateral quadrupole with preferential emission in the forward direction. The preferential emission in the forward direction, however, is hard to see. The peak sound occurs at about 30 deg, which is consistent with experimental observation (Troutt and McLaughlin,[40] Yamamoto et al.,[39] and Tanna[46]). However, the convection effect here (i.e., the predicted difference in forward and backward emission between 30 and 150 deg) is about 15 dB. The experimental observation (i.e., Yamamoto et al.[39]) is about 30 dB. (See also the same underprediction in Mankbadi and Liu.[21]) The present analysis is a straightforward application of Lighthill's integral in the spirit of Michalke and Fuchs[47] and Mankbadi and Liu[21] (i.e., working directly with the time-dependent source). The effects of refraction or sound-flow interactions are not accounted for herein. Several attempts (e.g., Ffowcs-Williams and Kempton[17]) were made to improve on Lighthill's original formulation. However, since the objective here is demonstrating the technique rather than comparing with experiment, no attempt to account for such effects on Lighthill's theory was considered herein.

We show partial spectra of the sound intensity for $\theta = 30$ deg in Fig. 20. The spectra indicate the peak at approximately $St = 1.55$. Tanna's[46] experimental observations show the peak at approximately $St = 1.5$. Application of Lighthill's theory herein is restricted to only the frequency modes that decay within the integration domain. This restriction is due to the oscillatory nature of the integration in Eq. (31) as illustrated in Fig. 21, which shows the absolute value of the integral in Eq. (31) as a function of the streamwise location where the integration is terminated. The value oscillates and becomes a constant only if the source term has decayed. Thus, the magnitude of sound intensity will be arbitrary, depending on the cutoff location, unless the computation is continued until the sound source has completely decayed. The importance of the compactness of the source and the convergence of Lighthill's integral was highlighted by Michalke.[48] Lighthill's stress tensor was represented by a simple wave. Michalke[48] showed that if the source is noncompact and its amplitude is constant in the downstream direction, the radiated sound will depend on the cutoff location. Further discussion on the effects of noncompactness are given by Michalke.[49] Thus, unless the computa-

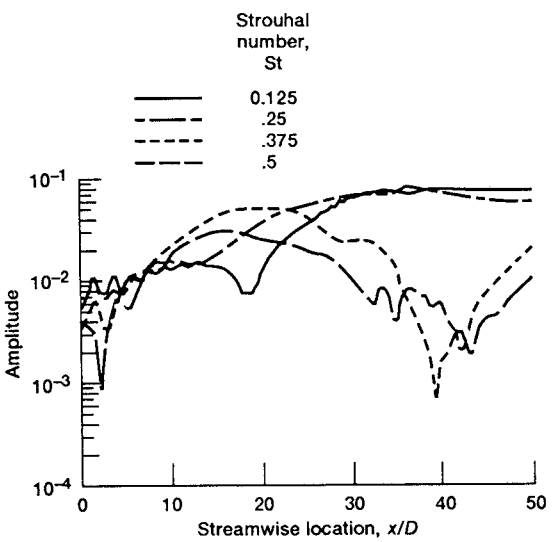

Fig. 16 Amplitude of harmonic disturbances.

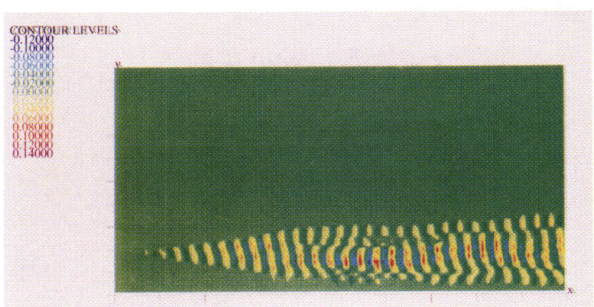

Fig. 17 Fourier transform of real part of ρuu.

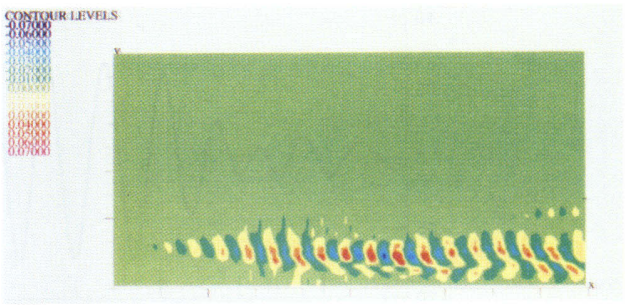

a) Real part

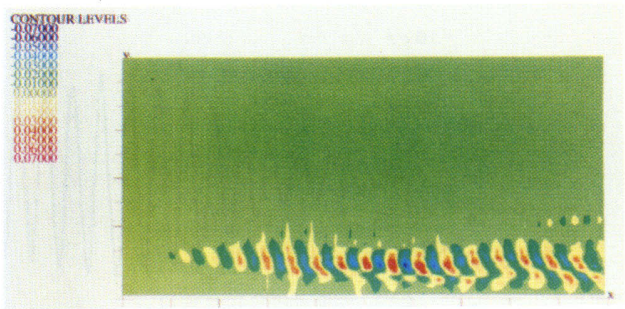

b) Imaginary part

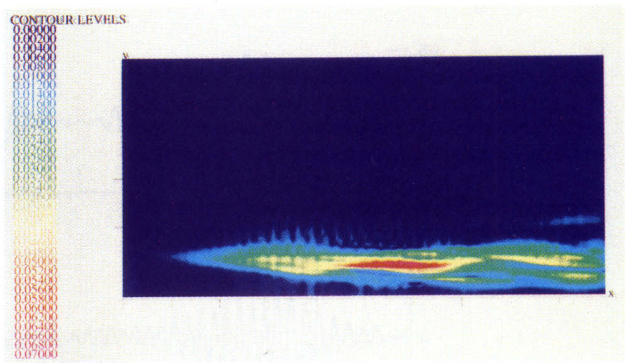

c) Absolute value

Fig. 18 Sound source at St = 0.5 as seen by observer at θ = 30 deg.

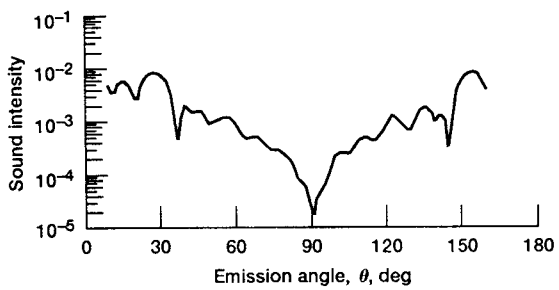

Fig. 19 Directivity of far-field sound for $St = 0.5$.

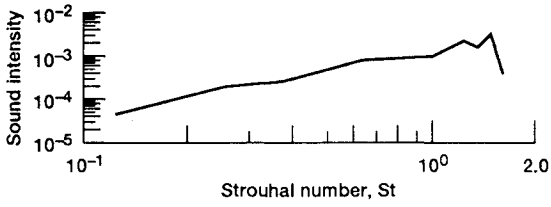

Fig. 20 Spectra of sound.

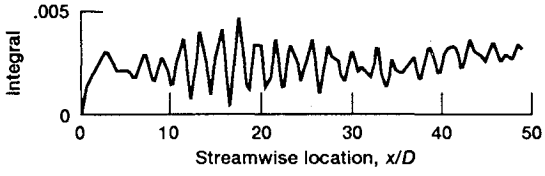

Fig. 21 Lighthill's integral as a function of streamwise truncation location.

tional domain extends far enough for the sound source to decay naturally, Lighthill's integral can be arbitrary. Because a large computational domain might not be practical, alternative approaches to Lighthill's theory may be needed. For instance Tam and Burton[50] attempted to work in the frequency domain and to match the near-field instability waves to the radiated sound through matched asymptotic expansion.

V. Discussion and Conclusions

Large-eddy simulations of a supersonic round jet were presented with emphasis on capturing the unsteady features of the flow. The sound source can thus be obtained directly from the calculated time field. The wavelike nature of the large-scale structure of a natural jet's time-dependent flowfield was demonstrated by taking the inflow disturbances to be completely random. Taking the inflow disturbances to be harmonic demonstrated how the large-scale structure can be enhanced and become more organized so that it resembles nonlinear instability waves. The disturbances in the Strouhal number range of 0–1.0 first amplified and subsequently decayed. The lower frequency modes peaked farther downstream, and the higher frequency ones peaked closer to the jet exit. Qualitative comparisons between results and observations indicate that indeed large-eddy simulations can be used as a tool for predicting the sound source from first principles. However, three-dimensional effects must be accounted for before quantitative comparisons with experimental results can be obtained.

The far-field sound can be obtained from the calculated time-dependent near field. It was shown that extending the solution domain far enough to directly obtain the sound field from Navier-Stokes equations requires prohibitive computer storage. To demonstrate how the calculated flowfield can be used to obtain the far-field sound, Lighthill's theory was used with the stress tensor obtained directly from the numerical simulations. The difficulties that arise from nonconvergence of the integral due to the noncompactness of the source were discussed. It may be impractical to extend the computational domain to capture the natural decay of the source. Alternatives to acoustics analogy will be considered in a subsequent work.

References

[1]Lighthill, M. J., "On Sound Generated Aerodynamically, Part I, General Theory," *Proceedings of the Royal Society of London, Series A: Mathematical and Physical Sciences*, Vol. 211, Feb. 7–March 20, 1952, pp. 564–587.

[2]Lilley, G. M., "On the Noise from Jets, Noise Mechanisms," *Noise Mechanics—AGARD Conference on Propagation and Reduction of Jet Noise*, AGARD CP 131, March 1974, pp. 13.1–13.12.

[3]Goldstein, M. E., "The Aeroacoustics of Turbulent Shear Flows," *Annual Review of Fluid Mechanics*, Vol. 16, Jan. 1984, pp. 263–285.

[4]Lighthill, M. J., "A General Introduction to Aeroacoustics and Atmospheric Sound," ICASE Rept. No. 92-52, NASA CR-189717, Oct. 1992.

[5]Bishop, K. A., Ffowcs-Williams, J. E., and Smith, W., "On the Noise Sources of Unsuppressed High Speed Jet," *Journal of Fluid Mechanics*, Vol. 50, Nov.-Dec. 1971, pp. 21–31.

[6]Crighton, D. G., "Acoustics as a Branch of Fluid Mechanics," *Journal of Fluid Mechanics*, Vol. 106, May 1981, pp. 261–298.

[7]Hussain, A. K. M. F., "Coherent Structures—Reality and Myth," *Physics of Fluids*, Vol. 26, No. 10, 1983, pp. 2816–2850.

[8]Hussain, A. K. M. F., "Coherent Structures and Turbulence," *Journal of Fluid Mechanics*, Vol. 173, Dec. 1986, pp. 303–356.

[9]Kibens, V., "Discrete Noise Spectrum Generated by an Acoustically Excited Jet," *AIAA Journal*, Vol. 18, No. 4, 1980, pp. 434–441.

[10]Liu, J. T. C., "Nonlinear Development of an Instability Wave in a Turbulent Wake," *Physics of Fluids*, Vol. 14, No. 10, 1971, pp. 2251–2257.

[11]Liu, J. T. C., "Developing Large-Scale Wavelike Eddies and the Near Jet Noise Field," *Journal of Fluid Mechanics*, Vol. 62, Jan.–Feb. 1974, pp. 437–464.

[12]Mollo-Christensen, E., "Jet Noise and Shear Flow Instability Seen From an Experimenter's Viewpoint," *Journal of Applied Mechanics*, Vol. 89, 1967, pp. 1–7.

[13]Zaman, K. B. M. Q., "Far-Field Noise of a Subsonic Jet Under Controlled Excitation," *Journal of Fluid Mechanics*, Vol. 152, March 1985, pp. 83–112.

[14]Zaman, K. B. M. Q., "Flow Field and Near and Far Sound Field of a Subsonic Jet," *Journal of Sound and Vibration*, Vol. 106, No. 1, 1986, pp. 1–16.

[15]Crighton, D. G., "Basic Principles of Aerodynamic Noise Generation," *Progress in Aerospace Sciences*, Vol. 16, 1975, pp. 31–96.

[16]Crow, S. C., "Acoustic Gain of a Turbulent Jet," American Physical Society Meeting (Boulder, CO), Paper IE6, Nov. 1972.

[17]Ffowcs-Williams, J. E., and Kempton, A. J., "The Noise from the Large-Scale Structure of a Jet," *Journal of Fluid Mechanics*, Vol. 84, Jan.-Feb. 1978, pp. 673–694.

[18]Liu, J. T. C., "Coherent Structure in Transitional and Turbulent Shear Flows," *Annual Review of Fluid Mechanics*, Vol. 21, Jan. 1989, pp. 285–315.

[19]Mankbadi, R. R., "Dynamics and Control of Coherent Structure in Turbulent Jets," *Applied Mechanics Review*, Vol. 45, No. 6, 1992, pp. 219–247.

[20]Tam, C. K. W., and Morris, P. J., "The Radiation of Sound by Instability Waves of a Compressible Plane Turbulent Shear Layer," *Journal of Fluid Mechanics*, Vol. 93, July–Aug. 1980, pp. 349–381.

[21]Mankbadi, R. R., and Liu, J. T. C., "Sound Generated Aerodynamically Revisited: Large-Scale Structures in a Turbulent Jet as a Source of Sound," *Philosophical Transactions of Royal Society of London, Series A: Mathematical and Physical Sciences*, Vol. 311, No. 183, 1984, pp. 183–217.

[22]Mankbadi, R. R., "The Self-Noise from Ordered Structures in a Low Mach Number Jet," *Journal of Applied Mechanics*, Vol. 57, March 1990, pp. 241–246.

[23]Michalke, A., "Survey on Jet Instability Theory," *Progress in Aerospace Sciences*, Vol. 21, 1984, pp. 159–199.

[24]Moin, P., Squires, K., Cabot, W., and Lee, S., "A Dynamical Subgrid-Scale Model for Compressible Turbulence and Scalar Transport," *Physics of Fluids A*, Vol. 3, No. 11, 1991, pp. 2746–2757.

[25]Tsuboi, K., Tamura, T., and Kuwahara, K., "Numerical Study of Vortex Induced Vibration of Circular Cylinder in High Reynolds Number Flow," AIAA Paper 89-0294, Jan. 1989.

[26]Hussaini, M. Y., Speziale, C. G., and Zang, T. A., "Discussion of the Potential and Limitations of Direct and Large-Eddy Simulations," NASA CR-181892, 1990.

[27]Smagorinsky, J., "General Circulation Experiments with the Primitive Equations. I. The Basic Experiment," *Monthly Weather Review*, Vol. 91, 1963, pp. 99–164.

[28]Erlebacher, G., Hussaini, M. Y., Speziale, C. G., and Zang, T. A., "Toward the Large-Eddy Simulation of Compressible Turbulent Flows," NASA CR-187460, 1990.

[29]Gottlieb, D., and Turkel, E., "Dissipative Two-Four Methods for Time-Dependent Problems," *Mathematics of Computation*, Vol. 30, No. 136, 1976, pp. 703–723.

[30]Farouk, B., Oran, E. S., and Kailasanath, K., "Numerical Simulations of the Structure of Supersonic Shear Layers," *Physics of Fluids A*, Vol. 3, No. 11, 1991, pp. 2786–2798.

[31]Ragab, S. A., and Sheen, S., "The Nonlinear Development of Supersonic Instability Waves in a Mixing Layer," *Physics of Fluids A*, Vol. 4, No. 3, 1991, pp. 553–566.

[32]Scott, J. N., Mankbadi, R. R., Hayder, M. E., and Hariharan, S. I., "Outflow Boundary Conditions for the Computational Analysis of Jet Noise," AIAA Paper No. 93-4366, Oct. 1993.

[33]Giles, M. B.,"Nonreflecting Boundary Conditions for Euler Equation Calculations," *AIAA Journal*, Vol. 28, No. 12, 1990, pp. 2050–2058.

[34]Tam, C. K. W., Webb, J. C., "Dispersion-Relation-Preserving Finite Difference Schemes for Computational Acoustics," *Journal of Computational Physics*, Vol. 107, No. 2, 1993, pp. 262–281.

[35]Thompson, K. W., "Time-Dependent Boundary Conditions for Hyperbolic Systems," *Journal of Computational Physics*, Vol. 68, No. 1, Jan. 1987.

[36]Seiner, J. M., and Norum, T. D., "Aerodynamic Aspects of Shock Containing Jet Plumes," AIAA Paper 80-0965, Oct. 1980.

[37]Scott, J. N., "Acoustic Analysis Using Numerical Solutions of Navier-Stokes Equations,", AIAA Paper 92-0506, Oct. 1992.

[38]Seiner, J. M., Ponton, M. K., Jansen, B. J., and Lagen, N. T., "The Effects of Temperature on Supersonic Jet Noise Emission," DGLR/AIAA Paper 92-02-046, Oct. 1992.

[39]Yamamoto, K. J., Brausch, J. F., Tanardan, B. A., Hoerst, D. J., Price, A. O., and Knott, P. R., "Experimental Investigation of Shock-Cell Noise Reduction for Single Stream Nozzles in Simulated Flight—Comprehensive Data Report," NASA CR-168234, 1984.

[40]Troutt, T. R., and McLaughlin, D. K., "Experiments on the Flow and Acoustic Properties of Moderate Reynolds Number Supersonic Jet," *Journal of Fluid Mechanics*, Vol. 116, March 1982, pp. 123–156.

[41]Drubka, R. R., Reisenthal, P., and Nagib, H. M., "The Dynamics of Low Initial Disturbance Turbulent Jets," *Physics of Fluids A*, Vol. 1, No. 10, 1989, pp. 1723–1735.

[42]Corke, T. C., and Kusek, S. M., "Resonance in Axisymmetric Jets with Controlled Helical Mode Input," AIAA Paper 91-0319, June 1991.

[43]Corke, T. C., Shakib, F., and Nagib, H. M., "Mode Selection and Resonant Phase Locking in Unstable Axisymmetric Jets," *Journal of Fluid Mechanics*, Vol. 223, Feb. 1991, pp. 253–311.

[44]Mankbadi, R. R., "On the Interaction Between Fundamental and Subharmonic Instability Waves in a Turbulent Round Jet," *Journal of Fluid Mechanics*, Vol. 160, Nov. 1985, pp. 385–419.

[45]Mankbadi, R. R., "Multifrequency Excited Jets," *Physics of Fluids A*, Vol. 3, No. 4, 1991, pp. 595–605.

[46]Tanna, H. K., "An Experimental Study of Jet Noise, Part I: Turbulent Mixing Noise," *Journal of Sound and Vibration*, Vol. 50, No. 3, 1977, pp. 405–428.

[47]Michalke, A., and Fuchs, H. V., "On Turbulence and Noise of an Axisymmetric Shear Flow," *Journal of Fluid Mechanics*, Vol. 70, July-Aug. 1975, pp. 179–205.

[48]Michalke, A., "A Wave Model for Sound Generation in Circular Jets," DFVLR, Rept. DLR-FB-70-57, Berlin, Feb. 1970.

[49]Michalke, A., "A Note on Non-Compact Acoustic Monopoles and Dipoles, *Journal of Sound and Vibration*, Vol. 17, No. 4, 1987, pp. 519–527.

[50]Tam, C. K. W., and Burton, D. E., "Sound Generated by Instability Waves of Supersonic Flows, Part 2: Axisymmetric Jets," *Journal of Fluid Mechanics*, Vol. 138, Jan. 1984, pp. 273–295.